EPJ Web of Conferences **259**, 11004 (2022) https://doi.org/10.1051/epjconf/202225911004
SQM 2021

System size and energy dependence of resonance production at ALICE

Vikash Sumberia[1] (**for the ALICE collaboration**)*

[1]University of Jammu, Jammu and Kashmir, 180006, India

Abstract. Hadronic resonances, thanks to their relatively short lifetimes, can be used to probe the properties of the hadronic phase in ultrarelativistic heavy-ion collisions. In particular their lifetimes are exploited to investigate the interplay between particle rescattering and regeneration after hadronization. In this contribution we present recent results on $\rho(770)^0$, $K^*(892)$, $\phi(1020)$, $\Sigma(1385)^{\pm}$, $\Xi(1530)^0$ and $\Lambda(1520)$ production in pp, p−Pb, Pb–Pb and Xe–Xe collisions at LHC energies.

1 Introduction

Production properties of hadronic resonances and their comparison with those of stable hadrons are useful tools to understand the properties of the strongly-interacting matter formed in relativistic nucleus-nucleus collisions. Due to their short lifetimes (comparable to the lifetime of the hadronic phase [1]), resonances provide an insight into the dynamical evolution of the fireball. The estimated yield of the resonances may be modified even after the chemical freezeout due to (pseudo)-elastic rescattering or regeneration of their decay daughters. These processes are dominant at low p_{T} ($\lesssim 2$ GeV/c) [2–4]. The rescattering process supresses the observed yields with respect to what is produced at chemical freeze-out while regeneration enhances the yield of resonances [5]. Thus, the study of resonance particles can provide an estimate for the lifetime of the hadronic phase (resonance to stable hadron yield ratios), understand the partonic in-medium energy losses (R_{AA} and R_{pA}) and the mechanism of particle production. In these proceedings, we present recent results obtained by ALICE for the mesonic resonances ($\rho(770)^0$, $\mathrm{K}(892)^{*0}$ and $\phi(1020)$) and baryonic resonances ($\Sigma(1385)^{\pm}$, $\Xi(1530)^0$ and $\Lambda(1520)$) in pp, p–Pb, Pb–Pb and Xe–Xe collisions at various centre-of-mass collision energies. Hereafter, the particles $\rho(770)^0$, $\mathrm{K}(892)^{*0}$, $\phi(1020)$, $\Sigma(1385)^{\pm}$ and $\Xi(1530)^0$ will be represented by ρ^0, K^{*0}, ϕ, $\Sigma^{\pm}$ and Ξ^0 respectively.

2 Analysis Method

This analysis used the data recorded by the ALICE detector [6]. The main components of ALICE which are relevant to these analyses are the Inner Tracking System (ITS, for tracking and vertex finding), Time Projection Chamber (TPC, for tracking and particle identification) and V0 detector (for triggering and centrality estimation). The events selected for the analysis are required to have a reconstructed primary vertex within 10 *cm* of the nominal interaction

*e-mail: vikash.sumberia@cern.ch

point along the beam direction (at the centre of the ALICE barrel). The measurements are performed at mid-rapidity ($|y| < 0.5$ in pp, Pb–Pb and Xe–Xe collisions and $0 < y_{cm} < 0.5$ in p–Pb collisions) and are presented as a function of charge particle density (which is also measured at mid-rapidity). The invariant mass is reconstructed from the measured momenta of identified particles. The combinatorial background is estimated using the event-mixing technique. The mixed-event distribution is then normalized to the unlike-charge distribution in the mass range $1.65 < M_{pK} < 1.75$ GeV/c^2 for $\Lambda(1520)$ (for details on other analyses see these citations [7–9, 11, 12]) and then subtracted from unlike-charge distribution in each p_{T} bin. The residual background is removed by fitting the invariant mass distribution with the sum of a Voigtian and a polynomial function. The raw yields are calculated after background subtraction and are corrected for finite detector acceptance, tracking efficiency of daughter particles and branching ratio. Table 1 shows the lifetime values, decay modes used for reconstruction and the branching ratios of some of the measured hadronic resonances.

Table 1: Lifetimes, reconstructed decay modes and branching ratios of measured resonance particles

	$\rho(770)^0$	$\mathrm{K}(892)^{*0}$	$\Sigma(1385)^{\pm}$	$\Lambda(1520)$	$\Xi(1530)^0$	$\phi(1020)$
Lifetime (fm/c)	1.3	4.2	5.5	12.6	21.7	46.4
Decay mode	$\pi^+\,\pi^-$	$\mathrm{K}^+\,\pi^-$	$\Lambda\,\pi^{\pm}$	$p\mathrm{K}^-$	$\Xi^-\,\pi^+$	$\mathrm{K}^+\,\mathrm{K}^-$
B.R. (%)	100	66.6	87.0	22.5	66.7	49.2

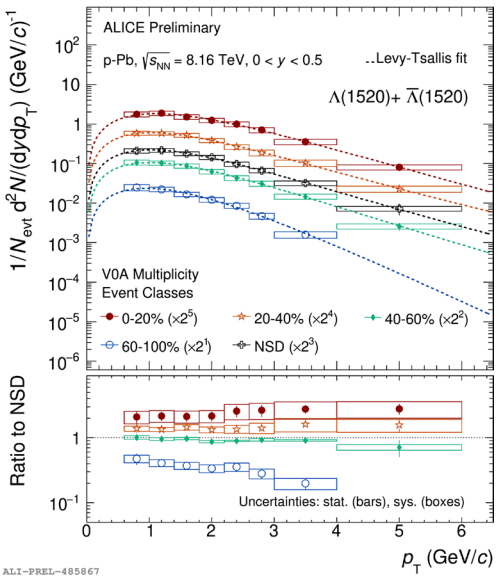

Figure 1. Corrected $\Lambda(1520)$ p_{T} spectrum for minimum-bias collisions (0–100%) and four multiplicity intervals (0–20%, 20–40%, 40–60% and 60–100%) in mid-rapidity p-Pb collisions at $\sqrt{s_{\mathrm{NN}}}$ =8.16 TeV. The errors shown here are both statistical (bars) and systematic (boxes). The shaded curves represent the Levy-Tsallis fit.

3 Results and discussion

We present new results on p_{T} spectra for $\Lambda(1520)$ resonance in p–Pb collisions in the mid-rapidity region at $\sqrt{s_{\mathrm{NN}}} = 8.16$ TeV in minimum-bias collisions (0-100 %) and four V0 event multiplicity classes (0–20%, 20–40%, 40–60% and 60–100%) as shown in Fig. 1. The minimum-bias spectra have been normalized to the fraction of non-single diffractive (NSD) events. We observed that p_{T} spectra harden with an increase in multiplicity and similar

behaviour is observed for other measured resonances in pp, p–Pb, Pb–Pb and Xe–Xe collisions [7–9].

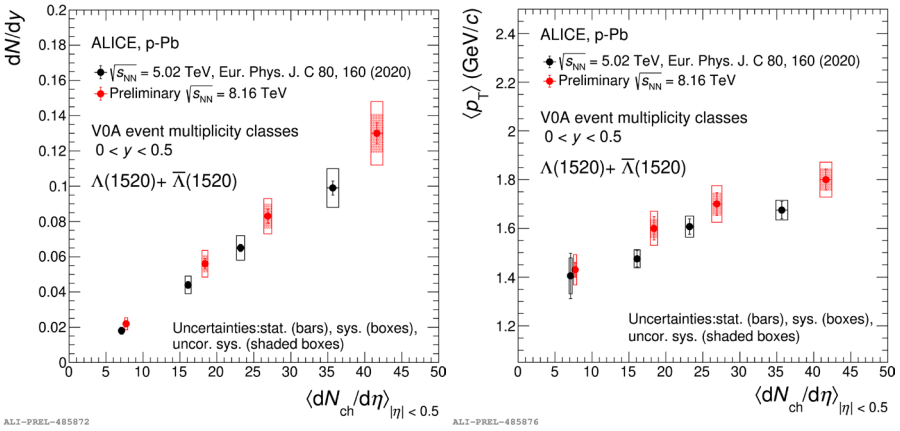

Figure 2: Integrated yield (left panel) and Average p_{T} (right panel) of $\Lambda(1520)$ in p–Pb collisions at $\sqrt{s_{\mathrm{NN}}}$ = 5.02 and 8.16 TeV in mid-rapidity region in various V0 event multiplicity classes. Bars show statistical errors, boxes show systematic errors and shaded boxes show uncorrelated errors.

The p_{T}-integrated yields of the $\Lambda(1520)$ in p–Pb collisons at $\sqrt{s_{\mathrm{NN}}}$ = 5.02 and 8.16 TeV (shown in the left panel of Fig. 2) have been measured in the mid-rapidity region in various V0 event multiplicity classes using the fitted Levy-Tsallis function to the measured p_{T} spectra of these resonances. Integrated yields of the resonances increase with event multiplicity and are independent of the colliding system and collision energy i.e. event multiplicity drives the resonance production. For the first time, average p_{T} of Λ^* in p–Pb collisions at $\sqrt{s_{\mathrm{NN}}}$ = 8.16 TeV is measured in mid-rapidity region for various V0 event multiplicity classes (shown in the right panel of Fig. 2). The results have been compared with the previous measurements in p–Pb at $\sqrt{s_{\mathrm{NN}}}$ = 5.02 TeV [10] and are comparable within the systematic uncertainties. The average p_{T} increases with event multiplicity.

The ratios of yields of resonances to those of stable hadrons is shown in the Fig. 3. We observe that the yields of ρ^0, K^{*0}, $\Sigma^{\pm}$, $\Lambda(1520)$ and Ξ^0 show a suppression with an increase in the centrality of Pb–Pb collisions, while no such suppression is seen in the ϕ resonance (due to its longer lifetime compared to the lifetime of hadronic phase). Different suppression of resonances, depending on their lifetimes, provide some evidence for the extraction of a lifetime of the hadronic phase. In small system collisions (pp and p–Pb), the yield suppression with increase in event multiplicity is only observed for ρ^0 and K^{*0} resonances. This shows the dependence of the lifetime of the hadronic phase on the colliding systems i.e. the lifetime of the hadronic phase increases with the increase in the size of the colliding system.

4 Conclusions

Recent results of the hadronic resonances $(\rho(770)^0$, $\mathrm{K}(892)^{*0}$, $\phi(1020)$, $\Sigma(1385)^{\pm}$, $\Lambda(1520)$ and $\Xi(1530)^0)$ in pp, p–Pb, Pb–Pb and Xe–Xe collisions obtained from the ALICE detector have been presented. The p_{T} spectra of these resonances get harder with the increase in multiplicity of the events. At similar event multiplicities resonance yields are independent of the colliding system or collision energy, which indicates that multiplicity drives the production

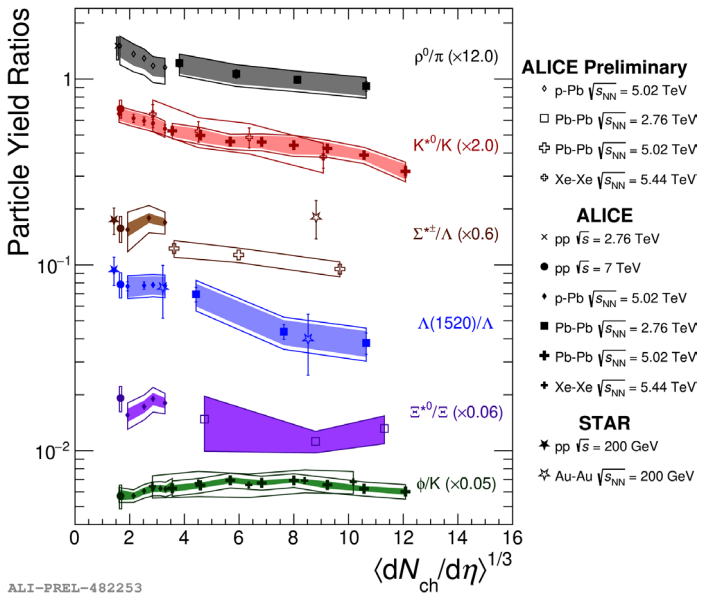

Figure 3: Ratios of integrated yields of various resonances to their respective stable particles in various systems and collision energies [13–18]. The bars and the boxes represent statistical and systematic uncertainty, respectively.

of resonance particles. The lifetime of the hadronic phase is limited (non-zero and finite) and this lifetime increases with the increase in the size of the colliding system.

References

[1] A. Aamodt *et al*. (ALICE Collaboration), Phys. Lett. B **696** , 328−37 (2011)
[2] Marcus Bleicher and Horst Stöcker, J. Phys. G **30** , S111−8 (2004)
[3] Markert C *et al*., AIP Conf. Proc. **631**, 533−52 (2002)
[4] Badalà Angela, EPJ Conf. Proc. **96**, 01003 (2015)
[5] S. A. Bass and A. Dumitru, Phys. Rev. C **61**, 064909 (2000)
[6] Aamodt K *et al*. (ALICE Collaboration), J. Inst. **3**, S08002 i-245 (2008)
[7] S. Acharya *et al*. (ALICE Collaboration) , Phys. Lett. B **802**, 135225 (2020)
[8] S. Acharya *et al*. (ALICE Collaboration) , Phys. Lett. B **807**, 135501 (2020)
[9] D. S. D. Albuquerque (ALICE Collaboration) , Nucl. Phys. A **982**, 823−826 (2019)
[10] S. Acharya *et al*. (ALICE Collaboration) , E. Phys. J. C **80**, 160 (2020)
[11] S. Acharya et al. (ALICE Collaboration) Phys. Rev. C **99**, 064901 (2019)
[12] J. Adam et al. (ALICE Collaboration) Eur. Phys. J. C **76**, 245 (2016)
[13] S. Acharya et al. (ALICE Collaboration) Phys. Rev. C **99**, 024906 (2019)
[14] D Adamova (ALICE Collaboration) Eur. Phys. J. C **77**, 389 (2017)
[15] D Adamova (ALICE Collaboration) Eur. Phys. J. C **75**, 1 (2015)
[16] Sevil Salur (Star Collaboration) NATO Science series **166**, S665-S667 (2004)
[17] S. Acharya et al. (ALICE Collaboration) Phys. Rev. C **99**, 024905 (2019)
[18] J. Adam et al. (ALICE Collaboration) Nat. Phys. **13**, 535-539 (2017)